HHS Public Access

Author manuscript

*J Control Release*. Author manuscript; available in PMC 2015 May 22.

Published in final edited form as:

*J Control Release*. 2012 November 28; 164(1): 49–57. doi:10.1016/j.jconrel.2012.09.021.

# Magnetic targeting of nanoparticles across the intact blood–brain barrier

**Seong Deok Kong**[a,1], **Jisook Lee**[b,1], **Srinivasan Ramachandran**[c], **Brian P. Eliceiri**[b], **Veronica I. Shubayev**[d], **Ratnesh Lal**[a,c,e], and **Sungho Jin**[a,c,*]

[a]Materials Science & Engineering, UC San Diego, La Jolla, CA 92093, USA

[b]Department of Surgery, School of Medicine, UC San Diego, San Diego, CA 92103, USA

[c]Department of Mechanical & Aerospace Engineering, UC San Diego, La Jolla, CA 92093, USA

[d]Department of Anesthesiology, School of Medicine, UC San Diego, La Jolla, CA 92093, USA

[e]Department of Bioengineering, UC San Diego, La Jolla, CA 92093, USA

## Abstract

Delivery of therapeutic or diagnostic agents across an intact blood–brain barrier (BBB) remains a major challenge. Here we demonstrate in a mouse model that magnetic nanoparticles (MNPs) can cross the normal BBB when subjected to an external magnetic field. Following a systemic administration, an applied external magnetic field mediates the ability of MNPs to permeate the BBB and accumulate in a perivascular zone of the brain parenchyma. Direct tracking and localization inside endothelial cells and in the perivascular extracellular matrix in vivo was established using fluorescent MNPs. These MNPs were inert and associated with low toxicity, using a non-invasive reporter for astrogliosis, biochemical and histological studies. Atomic force microscopy demonstrated that MNPs were internalized by endothelial cells, suggesting that trans-cellular trafficking may be a mechanism for the MNP crossing of the BBB observed. The silica-coated magnetic nanocapsules (SiMNCs) allow on-demand drug release via remote radio frequency (RF) magnetic field. Together, these results establish an effective strategy for regulating the biodistribution of MNPs in the brain through the application of an external magnetic field.

### Keywords

Blood; brain barrier; Magnetic; Drug delivery; Nanoparticles; Image analysis

## 1. Introduction

The blood–brain-barrier (BBB) represents an important physiological barrier that prevents effective targeting of the brain parenchyma with diagnostic and therapeutic agents. Targeting imaging molecules or therapeutic agents to the brain is a clinically important



*Corresponding author at: Department of Mechanical & Aerospace Engineering, UC San Diego, La Jolla, CA 92093, USA. jin@ucsd.edu (S. Jin).

[1]These authors contributed equally to this work.

problem yet technologies to alter their pharmaco-distribution have remained limited. For example, osmotic disruption of the BBB has been developed as a therapeutic strategy for the reversible opening of tight junctions, however these approaches can allow non-specific uptake of toxins in the brain [1]. Therefore, developing strategies for specific delivery of reagents across the intact BBB with minimal toxicity remains a challenge in the field.

Nanoparticle-based molecular transport has been the subject of recent strategies to enhance delivery and reduce toxicity [2–6] in diverse fields, including cardiology, hemostasis, ophthalmology, audiology, and oncology [7,8]. Magnetic nanoparticles in particular are actively being developed based on their unique properties to respond to magnetic fields including the well known magnetic hypothermia and controllable movements as well as their usage as an MRI contrast agent [9–13]. Moreover, the hydrodynamics of magnetic vectors have been extensively described and shown to exhibit well-defined physical characteristics [14] that enable the development of biologically compatible nanoparticles that can be evaluated in vivo. However, applications of magnetic nanoparticles to the brain have been more limited, due in part to a 30–50 cm working distance requirement for humans and FDA limitations of applied magnetic field strength on human subjects (8 T for adults, 4 T for children) [15]. Therefore, we have focused on the use of magnets to direct localization of MNPs with an enhanced magnetic design to meet these requirements. On the other hand, the capacity to control the spatial and temporal delivery of iron oxide particles with an external magnet has shown promise to address some of these limitations. However, most of these studies have focused on tumor-bearing rodent models [7,8,16], in which the normal BBB is already altered and the status of BBB integrity has remained poorly understood in terms of how the brain tumor barrier may facilitate or interfere with drug delivery [17]. Moreover, the precise location of the particles in reference to the vessels remain poorly understood at a cellular level.

Based on our previous experience with these MNPs in non-CNS tumor models to deliver chemotherapeutic agents [18], we have focused on the characterization of delivery of MNPs to the brain parenchyma of normal mice with intact BBB. First, we demonstrate the delivery of MNPs to the brain controlled by an external magnetic field with minimal neurotoxicity. Second, we reveal clear BBB crossing and extravasation of MNPs induced by external magnetic force using cellular level high-resolution imaging analysis in vivo. Third, we demonstrate the delivery of nanoparticles in the CNS crossing the intact BBB [19,20]. Together, our study establishes the capacity for the regulation of the CNS distribution of MNPs with the application of an external magnetic field, demonstrating crossing of the BBB and accumulation in the perivascular space with no apparent toxicity, which can be beneficial for treatments of CNS diseases.

## 2. Material and methods

### 2.1. General reagents

All reagents were purchased from Sigma-Aldrich, Inc. and Alfa Aesar, and used without further purification. The microscopy characterization of synthesized magnetic nanocapsules was carried out using a transmission electron microscope (FEI Tecnai G2 Sphera with 200 kV accelerated voltage) and a FEI field emission scanning electron microscope (Phillips

XL30 FEI SEM). Various chemical, magnetic and optical measurements were performed using SQUID magnetometer (Quantum Design MPMS2).

### 2.2. Synthesis of mono-disperse $Fe_3O_4$ nanoparticles/polystyrene composite nanospheres with a large volume fraction of trapped magnetite and fluorophores

Polystyrene nanospheres with trapped magnetic nanoparticles were prepared by combining mini-emulsion/emulsion polymerization technique according to the previous reported paper in our lab [18]. Briefly, a mixture of 24 g $FeCl_3 \cdot 6H_2O$ and 9.82 g $FeCl_2 \cdot 4H_2O$ was reacted with 50 mL of ammonium hydroxide under nitrogen gas at 80 °C, and then the solution was allowed to react for 1.5 h after the addition of 3.76 g of oleic acid. The magnetite nanoparticles so fabricated were washed with deionized water until neutral pH and then were transferred in situ in octane.

Magnetite and styrene mini emulsion containing 9,10-bis (phenylethynyl)anthracene were prepared using ultrasound and microporous glass membrane. With these emulsions, mono disperse $Fe_3O_4$/polystyrene nanospheres were synthesized with 40 mg potassium peroxydisulfate (KPS) at 80 °C for 20 h processing. The synthesized $Fe_3O_4$/polystyrene nanospheres were centrifuged and then were redispersed into 0.5% (wt/vol) polyoxyethylene sorbitan monolaurate aqueous solution. The suspension was added into 20 μL TEOS with 20 mL 2-propanol, and 0.5 mL ammonium hydroxide. The silica encapsulation reaction was performed at room temperature for 48 h. The resultant silica magnetic nanospheres were collected and washed by ethanol and water.

The procedure for fabrication of hollow capsules and subsequent loading of ibuprofen into SiMNCs followed the process that we reported previously [18].

### 2.3. Sample preparation for Atomic Force Microscope (AFM) analysis

Freshly cleaved mica substrate (12 mm diameter) was functionalized with a drop of Poly-L-Lysine (MW: 30 kDa) for a minute and rinsed thoroughly with MilliQ water. 50 μL of magnetic nanoparticle solution ($4\times10^{10}$particles/mL) was deposited on the mica substrate and allowed to adsorb for about 20 min at room temperature. After this incubation, the sample was gently washed in MilliQ water and imaged in Multimode AFM (Veeco Instruments) using a cantilever with a spring constant of 48 N/m, (NSC 11/50, Mikromasch) in tapping mode. A representative AFM image of the nanoparticles was flattened and plane fitted before carrying out particle analysis using Nanoscope Software (v5.31r1, Veeco Instruments). Multiple regions of the image were analyzed for the particle size distribution and the results tabulated.

### 2.4. Cell uptake studies

Human adult brain endothelial cell line (D3) was maintained in culture in EGM2-MV media (Lonza, MA) as described before [21]. 36 h before the experiments, cells were sub-cultured on glass bottom Petri dishes (MatTek Corp, MA) at 25,000 cells/$cm^2$. Prior to AFM imaging, cells were treated with magnetic nanoparticles at approximately 25 particles per cell and incubated for 4 h in the incubator. At the end of incubation, cells were thoroughly washed in warm HEPES buffered saline solution (5 times, 5 min each) to remove any free

particles from the cell surface. Cells were fixed in ice-cold methanol (−20 °C) on ice for 5 min and imaged in tapping mode in air using a Bioscope (Veeco Instruments).

### 2.5. Mice

10-week old mice were used for in vivo confocal imaging studies and biodistribution studies. GFAP-luc transgenic mice (FVB/N-Tg(Gfap-luc)) with the firefly luciferase gene under the control of 12 kb murine GFAP promoter were obtained from Caliper Life Sciences (Hopkinton, MA). At least 10-week old GFAP-luc mice were used for in vivo bioluminescent imaging. 2.4E9 fluorophore-labeled particles (resuspended in PBS, in 60–150 μL volume) were injected per mice for all in vivo experiments. To show that the nanoparticles move well in an aqueous solution. For example, in the presence of about 500 Oe applied field, the particles moved a distance of ~1.5 cm distance from a permanent magnet placed nearby [18]. The nanoparticles exhibit a superior magnetic vector with a movement speed of ~0.24 cm/s. The magnetic field is ~900 Oe at 1 cm distance and ~280 Oe at 2 cm distance. Nd–Fe–B disk-shaped magnet (1 inch diameter×1/2 inch thick, Dexter Magnetic Technologies with a magnetic field strength on the surface measured by gaussmeter of 6.3 KOe) was placed outside of the mouse skull on the surface of mouse skin or a Nd–Fe–B cylinder magnet (1/16 inch diameter×1/8 inch thick, K&J Magnetics, Inc. which exhibit a surface magnetic field of ~1.2 KOe) was implanted in mice brain by intracranial insertion to apply the magnetic field locally. All animal handling procedures were approved by the University of California San Diego Institutional Animal Care and Use Committee.

### 2.6. In vivo bioluminescent imaging

Astrogliosis was monitored before and following 1,2,4 h, 4 and 7 days after tail-vein injection of MNPs. Fur was removed from mice with electric clippers and Nair (Church & Dwight Co., Inc., Princeton, NJ) before imaging at each time point. Mice were injected through an intraperitoneal route with D-luciferin (150 μL of 15 mg/mL stock) and bioluminescent signals were assessed 10 min after D-luciferin injection over an integration time ranging from 2 s to 1 min using a cooled charge-coupled device (CCD) camera (Spectrum; Caliper Life Sciences, Hopkinton, MA) capable of in vivo imaging. GFAP-activity was monitored by quantitation of light emission from a region of interest drawn over the brain at each time point (Unit = radiance). Bioluminescent signal from the ear represents basal level of GFAP activity and was excluded from the ROI. Images were analyzed using Living Image software version 4.0 (Caliper Life Sciences, Hopkinton, MA).

### 2.7. Body distribution of MNPs

Mice were injected with fluorophore-labeled MNPs intravenously. 1, 2, and 4 h post-injection, brain, liver, spleen and kidney were harvested. Fluorescent signals from organs were measured with cooled charge-coupled device (CCD) camera (Spectrum; Caliper Life Sciences, Hopkinton, MA) using a 675-nm excitation and a 720-nm emission filter.

### 2.8. Confocal microscopy

Mice were injected with fluorophore-labeled MNPs intravenously. One hour post-injection, brains were harvested and 1 mm brain sections were made. Thick brain sections were imaged with an Olympus Fluoview 1000 (ASW 1.7b) laser scanning confocal microscope (LSCM) (Olympus, Melville, NY) equipped with 10×/0.4 N.A. and 20×/0.7 N.A. dry objective lenses on a BX61 microscope (Olympus). Brain sections were fixed with 10% formalin and were subjected to hematoxylin and eosin staining after confocal analysis.

### 2.9. Immunofluorescence

Ten-μm-thick brain or nerve sections were immersed in 0.5% sodium borohydride followed by antigen retrieval and nonspecific binding block as described above, then primary rabbit anti-cleaved caspase 3 antibody (Cell Signaling, Danvers, MA) mouse anti-GFAP (Cell Signaling), or rabbit anti-Iba-1 (Wako, Richmond, VA), incubation overnight at 4 °C, followed by goat anti-rabbit 594 (red) or 488 (green) Alexa for 1 h. Sections were mounted using Slowfade gold antifade reagent (Molecular Probes). Imaging was performed using a Leica DMR bright-light and fluorescent microscope and Openlab 4.04 imaging software (Improvision Inc., Waltham, MA).

### 2.10. Western blotting

Tissues were isolated 4 weeks after the i.v. MNP injection, frozen in liquid nitrogen, and stored at −80 °C until analyzed. Proteins were extracted using lysis buffer (50 mM Tris–HCl, pH 7.4, 1% NP 40, 150 mM NaCl, 1 mM EDTA, 1 mM PMSF, 1 μg/mL aprotinin and leupeptin, 1 mM sodium orthovanadate). 100 μg of total protein, as detected by BCA Protein Assay (Pierce, Rockford, IL), was separated on 10% Tris–glycine SDS-PAGE (Bio-Rad, Hercules, CA) at 50 to 80 mA, and transferred to nitrocellulose using iBlot dry blotting system (Invitrogen) at 20 V for 7 min. The membranes were blocked with 5% non-fat milk (Bio-Rad). A primary antibody to phosphorylated extracellular signal-regulated kinases (pERK1/2), total ERK1/2 or caspase 3, all raised in rabbit and obtained from Cell Signaling Technology were diluted in 5% bovine serum albumin and applied overnight at 4 °C. The membranes were washed in TBS containing 0.05% Tween and incubated for 1 h at room temperature with HRP-conjugated anti-rabbit secondary antibody (Cell Signaling Technology) and developed using an enhanced chemiluminescence (ECL, Amersham).

### 2.11. In vitro remote activated drug release measurement

After Ibuprofen (Ibp)-loaded SiMNCs were prepared, the remote RF activated drug release was measured by UV/VIS spectrophotometer. For the first 10 min, the solution containing fresh 1 mL PBS was left without RF and then the Ibp release was measured. After the measured solution was replaced with a fresh 1 mL PBS, the solution was exposed to RF (at 100 kHz) for 30 s. After the Ibp supernatants were cleared of floating particles, the drug contents were measured using UV/VIS absorption for the dissolved drug in the solution. After the switch “ON” measurement was done, SiMNCs were re-suspended in the fresh 1 mL PBS again, and then the solution was left for 5 min without RF. Next, after waiting for 5 min of “off” time, the drug content in the solution was measured by UV/VIS

spectrophotometer. The switch “ON–OFF” measurements were taken alternately and the release profile was graphed.

### 2.12. Statistical analysis

Error bars in Figs. 2(A), (C), and 3(B) represent standard deviation. Error bars in Fig. 4(B) represent standard error of the mean.

Statistical analysis was performed using Mstat software (version 5.10; N. Drinkwater, McArdle Laboratory for Cancer Research, School of Medicine and Public Health, University of Wisconsin, which is available for downloading at http://www.mcardle.wisc.edu/mstat/).

## 3. Results

### 3.1. Characterization of fluorophore labeled MNPs

To image MNPs, we developed fluorophore-embedded nanoparticles of ~100 nm diameter using a modified emulsion process [22]. Fig. 1 shows representative micrographs and fluorescent images of MNPs labeled with 9,10-bis(phenylethynyl)anthracene, by laser scanning confocal microscopy (LSCM) (Fig. 1C). The M–H magnetization loop of the MNPs was compared with the free iron oxide particles of same individual particle size (~10 nm) (Fig. 1D).

We observed that MNPs provided substantially improved magnetization (~5 times higher at 500 Oe) compared to typical super-paramagnetic iron oxide nanoparticles. This was attributed to their close proximity and tighter interaction of magnetic particles in the confined geometry of polystyrene particles resulting in the higher magnetization and enhanced response to applied magnetic field.

### 3.2. Biodistribution of MNPs

To assess the delivery and kinetics of MNP accumulation in the brain parenchyma we first performed LSCM imaging on brains of mice that have been subjected to an intravenous injection of fluorescent MNPs in the absence of an external magnetic field. MNPs were detected in the brain as early as 5 min after intravenous injection (data not shown), and reached a steady-state at 30 to 120 min post-injection, which was 10-fold higher than background (Fig. 2A).

We did not observe any preferential accumulation of MNPs within the brain in the absence of applied magnetic field (data not shown). A large fraction of MNPs was cleared from the circulation mostly by the liver and some by the spleen (Fig. 2B,C, Supplementary Fig. 1) within 1 h, however, at least 30% of the maximum signal was still detectable in the brain 48 h post-injection (Fig. 2A). These studies demonstrate the retention of a baseline level of MNPs in the brain parenchyma.

### 3.3. Magnetically vectored MNPs accumulate in the brain

To assess the magnetic properties and responsiveness of MNPs to the external magnetic field applied locally, a Nd–Fe–B magnet was implanted in the right hemisphere of mouse

cerebral cortex in vivo as described in the Materials and methods section. One-week post-implantation, MNPs were delivered systemically by intravenous injection followed by LSCM imaging analysis to track their distribution in the brain. As expected, MNPs were enriched in the ipsilateral hemisphere where the magnet was implanted compared to the contralateral hemisphere (Fig. 3A). Within the ipsilateral hemisphere, accumulation of MNPs was observed in the cortex near the magnet, whereas areas farther from the magnet displayed lower accumulation (Fig. 3B). Histological analysis using hematoxylin and eosin staining confirmed a large accumulation of MNPs in the vessels of the ipsilateral hemisphere. The fields shown were distal to the implantation site where there was non-specific MNPs observed due to implantation site-induced injury (data not shown). These results indicate that spatial distribution of MNPs can be controlled by the application of an external magnetic field.

### 3.4. External magnetic force enhances BBB crossing and perivascular accumulation of MNPs in the brain

To avoid the tissue damage caused by the invasive magnet implantation in the brain, we tested whether the distribution of MNPs could be altered by the application of noninvasive, external magnetic field (estimated to be ~1000 Oe [18], applied by placing a Nd–Fe–B magnet near the mouse head using an immobilized tube apparatus). Using 1 h as a time point with steady state kinetics (Fig. 2A), we assessed the distribution of systemically delivered MNPs. We observed a ~25-fold increase in brain retention with the application of the magnet compared to a no-magnet control (Fig. 4B). In animals exposed to the magnet, we observed more heterogeneity in fluorescent MNPs compared with sham mice without a magnet, which likely represented signal from clusters of MNPs (Fig. 4A). In the absence of applied magnetic field, majority of MNPs were localized within the capillaries with few MNPs observed outside the microvessel environment based on histology and unpublished observations. Following the application of external magnetic field, there was an increase in the crossing of MNPs across the BBB into the perivascular space and parenchyma (Fig. 4C, arrows). Importantly, we did not observe any histological changes suggesting that the blood vessels where the particles were found were intact (Fig. 4C). To further characterize MNP distribution with respect to BBB, we performed LSCM image analysis of fluorescent MNPs in mice that had been subjected to a systemic injection of TRITC-labeled 70 kDa fluorescent dextran with a magnet as an indication of BBB integrity and localization of brain capillaries.

Consistent with the histological findings, MNPs were detected in both blood vessels and in the perivascular extracellular matrix (ECM), but no TRITC–dextran was detected in the perivascular space (Fig. 4D). These results suggest that the application of external magnetic field facilitated MNPs to cross the BBB with no apparent damage to its integrity.

### 3.5. MNP administration produced no acute or long-term toxicity in vivo

Hierarchical oxidative stress is the main predictive toxicological paradigm for the assessment of nanomaterial hazards [6,23–27]. As such, it involves an incremental series of cellular responses, which after the initial defensive antioxidant response (Tier 1), can lead to extended immunotoxicity (Tier 2) and cytotoxicity/apoptosis (Tier 3). We have previously used a transgenic mouse model expressing the firefly luciferase reporter gene under the

control of the glial fibrillar acidic protein (GFAP-luc) [22] to assess neurotoxicity and astrogliosis following CNS [28–30] and BBB breakdown [31]. We used a similar strategy to assess astrogliosis, as a feature of immunotoxicity in this study. Following intravenous administration of MNPs into GFAP-luc mice, we observed a slight increase in the GFAP activity 1 day after injection compared with the baseline signal. However, the signal decreased by day 4 and returned close to baseline on day 7 (Fig. 5A,B), indicating that the activation of GFAP by accumulated MNPs is reversible and did not induce a long-term effect at the concentration used in the study. Potential toxicity of MNPs was further assessed in brain sections (Fig. 5C) and tissue lysates of brain, liver and spleen (Fig. 5D), as the major organs accumulating MNPs.

We observed that neither the activation of the mitogen-activated protein kinases, p38, JNK and ERK1/2 (ERK1/2 is shown in Fig. 5) nor of caspase 3 (17 kDa cleavage product) was elevated in the brain, liver or spleen 4-weeks after MNP injection. These assays suggest that MNP administration produced no extended immunotoxicity or cell death in these organs in vivo.

### 3.6. MNPs uptake by endocytosis into human brain endothelial cells

To understand the cellular uptake of MNPs, we imaged human brain endothelial cells treated with MNPs with atomic force microscopy (AFM) [32]. AFM imaging demonstrated that MNPs were spherical in shape with an average diameter of 124 nm (Fig. 6A,B). To understand the possible mechanism of how MNPs can cross the BBB in vivo, we tested if these particles can internalize into brain endothelial cells that maintain the barrier properties of BBB. In vitro cellular uptake study revealed multiple intracellular granular structures distributed across the entire cell cytoplasm, with a peri-nuclear localization demonstrating their efficient uptake into human endothelial cells (Fig. 6C). The particle sizes inside the cells (>800 nm) suggested that the MNPs were clustered. Together, these results suggest that endothelial cell membrane-mediated translocation of MNPs may be a mechanism for the BBB crossing observed in vivo. These studies support a model for the use of external magnets to direct the distribution of MNPs for in vivo models where delivery across an intact BBB is advantageous (Fig. 6D).

### 3.7. On-demand drug release from silica-coated magnetic nanocapsules (SiMNCs)

To achieve on-demand drug release from drug-containing SiMNCs, switchable on–off release of Ibp, an amyloid-binding molecule [33], was enabled by applying a RF field to the SiMNCs. The ibuprofen was loaded to the interior of the hollow SiMNCs, and the drug release was controlled via activation of remote RF magnetic field (at 100 kHz). Shown in Fig. 7A are ~150 nm diameter, hollow silica nanospheres with retained magnetic nanoparticles. In Fig. 7B, a dramatic change in the amount of released drug is observed when the remote magnetic field is switched “on” and “off”.

## 4. Discussion

We have designed and developed fluorescent MNPs and demonstrated their ability in vivo to access the brain parenchyma by crossing the normal BBB under the regulation of an external

magnetic field. While the mechanism of BBB crossing remains unknown, our data indicate that the endothelial membrane is capable of MNP uptake with kinetics that is consistent with the in vivo model. Our AFM results show that these MNPs are spherical in shape with an average diameter of ~124 nm, which enables efficient uptake by human brain endothelial cells. The fluorescence of the MNPs enables their direct tracking and localization within specific vascular niches in the brain. Furthermore, the enhanced magnetic property and their responsiveness to an external magnetic field to facilitate their extravasation and/or accumulation in the brain parenchyma supports the idea of application of similarly configured, drug-containing magnetic nanocapsules [28–30,34,35] to deliver CNS drugs across an intact BBB. We demonstrate in this study the increased sensitivity to a magnetic field of engineered MNPs compared to standard magnetic nanoparticles, and explore the capacity to use such MNPs to access the brain parenchyma.

We have focused on delivery across the intact BBB. Recent studies also demonstrate the usage of external magnetic field to facilitate the delivery of MNPs across the BBB [34,36]. In addition to these reports, our research demonstrates BBB translocation of MNPs with higher resolution confocal analysis to pinpoint the extravasation of MNPs in reference to the vasculature, which is supported by our histological analysis. Furthermore, unlike in vitro BBB cell culture models with limitations, our in vivo model is more suitable to study the multi-cellular complex nature of BBB and pharmacodistribution of MNPs. Moreover, our data indicate that magnet-mediated delivery of MNPs can occur in normal brain parenchyma without any vascular leak as observed with the TRITC–70 kDa dextran. The internalization of MNPs observed by the AFM imaging indicates that endocytosis or a non-specific membrane-mediated uptake of the MNPs occurs, the mechanism underlying such uptake is unclear and beyond the scope of this study. Nevertheless, the critical conclusion of these studies is that MNP uptake into the brain does not appear to require a major disruption of the endothelial barrier or alteration in BBB integrity. Based on the capacity to load such MNCs with drugs and the cell biological analysis with respect to BBB integrity, these MNPs are ideal candidates to examine their relevance in translational models.

The importance of understanding the potential for toxic effects both at systemic and local levels in terms of translational development cannot be understated. Therefore, we deployed the assessment of oxidative stress, focusing on inflammatory changes (Tier 2) that set after the exposed tissues attempt to restore redox equilibrium during Tier 1, and on the highest level of oxidative stress (Tier 3), when interference in lysosomal and mitochondrial functions can lead to apoptosis, as a final common pathway of nanotoxicity [23,24]. In particular, we focused on changes in cellular membranes (i.e. AFM studies), vascular leak (i.e. TRITC–dextran), effects on neuroinflammation and astrogliosis (i.e. GFAP-luc reporter), inflammation signaling (i.e. ERK1/2 phosphorylation) and apoptosis (i.e. caspase 3 cleavage) in major organs that internalized MNPs. It remains unknown if MNPs induce substantial tissue remodeling or oxidative stress injury in other tissues or times-points after their systemic delivery. In contrast, we observe that high doses of iron oxide nanoparticles of known toxic potential [37] directly inoculated into the nervous system, have the capacity to activate ERK1/2 and caspase 3. Further investigations will be necessary to assess the effect of MNP on activating other, less common, signaling pathways of nanoparticle toxicity and in the conditions associated with the leaky BBB.

Unlike other targeted delivery methods, (such as one mediated by antibodies to specific cell surface receptors), magnetically mediated translocation of MNPs does not appear to induce deleterious signal transduction events and exhibits minimal accumulation in other organs [38]. Accumulation of particles to a specific region of the body could be regulated by changing their exposure to the applied magnetic field and shape of the magnet, thus minimizing the toxicity. Together, the enhanced magnetic properties of iron oxide particles in the nanocapsule configuration and the capacity to use external magnet to alter their penetration and distribution in the brain parenchyma non-invasively has great potential for usage in the treatment of brain diseases.

## 5. Conclusions

We have successfully created MNPs of 100 nm size, which provide powerful magnetic vector for BBB crossing. These nanoparticles containing a fluorophore within have been engineered for direct tracking and measurement of the position of MNPs, which also allow cellular-level high-resolution imaging analysis such as confocal microscopy. Applied magnetic field facilitated the extravasation and/or accumulation of these magnetic nanoparticles in the brain parenchyma. Similarly configured, but drug-containing magnetic nanocapsules can be utilized for BBB crossing and treatment of various CNS diseases.

## Supplementary Material

Refer to Web version on PubMed Central for supplementary material.

## Acknowledgments

The authors acknowledge financial support by the Iwama Fund at UC San Diego (SJ), NSF through Grant No. DMR-1006081 (SDK, SJ), NIH R01-HL073396 (BPE), the American Brain Tumor Association (JL) and NIH R21-ES015871 (VIS) and the Mechanical and Aerospace Engineering and Bioengineering Departmental Developmental Fund (RL).

## Appendix A. Supplementary data

Supplementary data to this article can be found online at http://dx.doi.org/10.1016/j.jconrel.2012.09.021.

## References

1. Neuwelt EA, Bauer B, Fahlke C, Fricker G, Iadecola C, Janigro D, Leybaert L, Molnár Z, O'Donnell ME, Povlishock JT, Saunders NR, Sharp F, Stanimirovic D, Watts RJ, Drewes LR. Engaging neuroscience to advance translational research in brain barrier biology. Nat Rev Neurosci. 2011; 12:169–182. [PubMed: 21331083]
2. Vauthier C, Labarre D, Ponchel G. Design aspects of poly(alkylcyanoacrylate) nanoparticles for drug delivery. J Drug Target. 2007; 15:641–663. [PubMed: 18041633]
3. Kreuter J. Nanoparticulate systems for brain delivery of drugs, Adv. Drug Deliv Rev. 2001; 47:65–81.
4. Kreuter J, Shamenkov D, Petrov V, Ramge P, Cychutek K, Koch-Brandt C, Alyautdin R. Apolipoprotein-mediated transport of nanoparticle-bound drugs across the blood–brain barrier. J Drug Target. 2002; 10:317–325. [PubMed: 12164380]
5. Olivier JC. Drug transport to brain with targeted nanoparticles. NeuroRx. 2005; 2:108–119. [PubMed: 15717062]

6. Shubayev VI, Pisanic TR, Jin S. Magnetic nanoparticles for theragnostics. Adv Drug Deliv Rev. 2009; 61:467–477. [PubMed: 19389434]
7. Hua MY, Liu HL, Yang HW, Chen PY, Tsai RY, Huang CY, Tseng IC, Lyu LA, Ma CC, Tang HJ, Yen TC, Wei KC. The effectiveness of a magnetic nanoparticle-based delivery system for BCNU in the treatment of gliomas. Biomaterials. 2011; 32:516–527. [PubMed: 21030073]
8. Chertok B, David AE, Yang VC. Brain tumor targeting of magnetic nanoparticles for potential drug delivery: effect of administration route and magnetic field topography. J Control Release. 2011; 155:393–399. [PubMed: 21763736]
9. Alexiou C, Arnold W, Klein RJ, Parak FG, Hulin P, Bergemann C, Erhardt W, Wagenpfeil S, Lübbe AS. Locoregional cancer treatment with magnetic drug targeting. Cancer Res. 2000; 60:6641–6648. [PubMed: 11118047]
10. Reiss G, Hutten A. Magnetic nanoparticles are useful for a wide range of applications from data storage to medicinal imaging. The large-scale preparation of FeCo nanoparticles boosts this potential. Nat Mater. 2005; 4:725–726. [PubMed: 16195762]
11. Qiao R, Jia Q, Hüwel S, Xia R, Liu T, Gao F, Galla H, Gao M. Receptor-mediated delivery of magnetic nanoparticles across the blood–brain barrier. ACS Nano. 2012; 6:3304–3310. [PubMed: 22443607]
12. Dilnawaz F, Singh A, Mohanty C, Sahoo SK. Dual drug loaded superparamagnetic iron oxide nanoparticles for targeted cancer therapy. Biomaterials. 2010; 31:3694–3706. [PubMed: 20144478]
13. Ma Y, Wu S, Wu T, Chang Y, Hua M, Chen J. Magnetically targeted thrombolysis with recombinant tissue plasminogen activator bound to polyacrylic acid-coated nanoparticles. Biomaterials. 2009; 30:3343–3351. [PubMed: 19299010]
14. Voltairas PA, Fotiadis DI, Michalis LK. Hydrodynamics of magnetic drug targeting. J Biomech. 2002; 35:813–821. [PubMed: 12021001]
15. Shapiro B, Dormer K, Rutel IB. A two-magnet system to push therapeutic nanoparticles. AIP Conf Proc. 2010; 1311:77–88. [PubMed: 21243119]
16. Dilnawaz F, Singh A, Mewar S, Sharma U, Jagannathan NR, Sahoo SK. The transport of non-surfactant based paclitaxel loaded magnetic nanoparticles across the blood brain barrier in a rat model. Biomaterial. 2012; 33:2936–2951.
17. Lockman PR, Mittapalli RK, Taskar KS, Rudraraju V, Gril B, Bohn KA, Adkins CE, Roberts A, Thorsheim HR, Gaasch JA, Huang S, Palmieri D, Steeg PS, Smith QR. Heterogeneous blood-tumor barrier permeability determines drug efficacy in experimental brain metastases of breast cancer. Clin Cancer Res. 2010; 16:5664–5678. [PubMed: 20829328]
18. Kong SD, Zhang W, Lee JH, Brammer K, Lal R, Karin M, Jin S. Magnetically vectored nanocapsules for tumor penetration and remotely switchable on-demand drug release. Nano Lett. 2010; 10:5088–5092. [PubMed: 21038917]
19. Diop-Frimpong B, Chauhan VP, Krane S, Boucher Y, Jain RK. Losartan inhibits collagen I synthesis and improves the distribution and efficacy of nanotherapeutics in tumors. Proc Natl Acad Sci U S A. 2011; 108:2909–2914. [PubMed: 21282607]
20. Lee J, Borboa AK, Chun HB, Baird A, Eliceiri BP. Conditional deletion of the focal adhesion kinase FAK alters remodeling of the blood–brain barrier in glioma. Cancer Res. 2010; 70:10131–10140. [PubMed: 21159635]
21. Weksler BB, Subileau EA, Perriere N, Charneau P, Holloway K, Leveque M, Tricoire-Leignel H, Nicotra A, Bourdoulous S, Turowski P, Male DK, Roux F, Greenwood J, Romero IA, Couraud PO. Blood–brain barrier-specific properties of a human adult brain endothelial cell line. FASEB J. 2005; 19:1872–1874. [PubMed: 16141364]
22. Zhu L, Ramboz S, Hewitt D, Boring L, Grass DS, Purchio AF. Non-invasive imaging of GFAP expression after neuronal damage in mice. Neurosci Lett. 2004; 367:210–212. [PubMed: 15331155]
23. Meng H, Xia T, George S, Nel AE. A predictive toxicological paradigm for the safety assessment of nanomaterials. ACS Nano. 2009; 3:1620–1627. [PubMed: 21452863]

24. Rallo R, France B, Liu R, Nair S, George S, Damoiseaux R, Giralt F, Nel A, Bradley K, Cohen Y. Self-organizing map analysis of toxicity-related cell signaling pathways for metal and metal oxide nanoparticles. Environ Sci Technol. 2011; 45:1695–1702. [PubMed: 21250674]
25. Nel A, Xia T, Madler L, Li N. Toxic potential of materials at the nanolevel. Science. 2006; 311:622–627. [PubMed: 16456071]
26. Oberdorster G, Oberdorster E, Oberdorster J. Nanotoxicology: an emerging discipline evolving from studies of ultrafine particles. Environ Health Perspect. 2005; 113:823–839. [PubMed: 16002369]
27. Dobrovolskaia MA, McNeil SE. Immunological properties of engineered nanomaterials. Nat Nanotechnol. 2007; 2:469–478. [PubMed: 18654343]
28. Pekny M, Nilsson M. Astrocyte activation and reactive gliosis. Glia. 2005; 50:427–434. [PubMed: 15846805]
29. Sofroniew MV. Molecular dissection of reactive astrogliosis and glial scar formation. Trends Neurosci. 2009; 32:638–647. [PubMed: 19782411]
30. Eddleston M, Mucke L. Molecular profile of reactive astrocytes—implications for their role in neurologic disease. Neuroscience. 1993; 54:15–36. [PubMed: 8515840]
31. Maysinger D, Behrendt M, Lalancette-Hebert M, Kriz J. Real-time imaging of astrocyte response to quantum dots: in vivo screening model system for biocompatibility of nanoparticles. Nano Lett. 2007; 7:2513–2520. [PubMed: 17638392]
32. Ramachandran S, Quist AP, Kumar S, Lal R. Cisplatin nanoliposomes for cancer therapy: AFM and fluorescence imaging of cisplatin encapsulation, stability, cellular uptake, and toxicity. Langmuir. 2006; 22:8156–8162. [PubMed: 16952256]
33. Capule CC, Yang J. Enzyme-linked immunosorbent assay-based method to quantify the association of small molecules with aggregated amyloid peptides. Anal Chem. 2012; 84:1786–1791. [PubMed: 22243436]
34. Saiyed ZM, Gandhi NH, Nair MP. Magnetic nanoformulation of azidothymidine 5′-triphosphate for targeted delivery across the blood–brain barrier. Int J Nanomedicine. 2010; 5:157–166. [PubMed: 20463931]
35. Liu HL, Hua MY, Yang HW, Huang CY, Chu PC, Wu JS, Tseng IC, Wang JJ, Yen TC, Chen PY, Wei KC. Magnetic resonance monitoring of focused ultrasound/magnetic nanoparticle targeting delivery of therapeutic agents to the brain. Proc Natl Acad Sci U S A. 2010; 107:15205–15210. [PubMed: 20696897]
36. Han L, Zhang A, Wang H, Pu P, Kang C, Chang J. Construction of novel brain-targeting gene delivery system by natural magnetic nanoparticles. J Appl Polym Sci. 2011; 121:3446–3454.
37. Pisanic, T.; Jin, S.; Shubayev, VI. Iron oxide magnetic nanoparticle nanotoxicity: incidence and mechanisms. In: Sahu, SC.; Casciano, DA., editors. Nanotoxicity: From Health Risk to In Vitro and In Vivo Models. John Wiley & Sons Ltd; 2009. p. 397-425.
38. Tosi G, Vergoni AV, Ruozi B, Bondioli L, Badiali L, Rivasi F, Costantino L, Forni F, Vandelli MA. Sialic acid and glycopeptides conjugated PLGA nanoparticles for central nervous system targeting: in vivo pharmacological evidence and biodistribution. J Control Release. 2005; 145:49–57. [PubMed: 20338201]

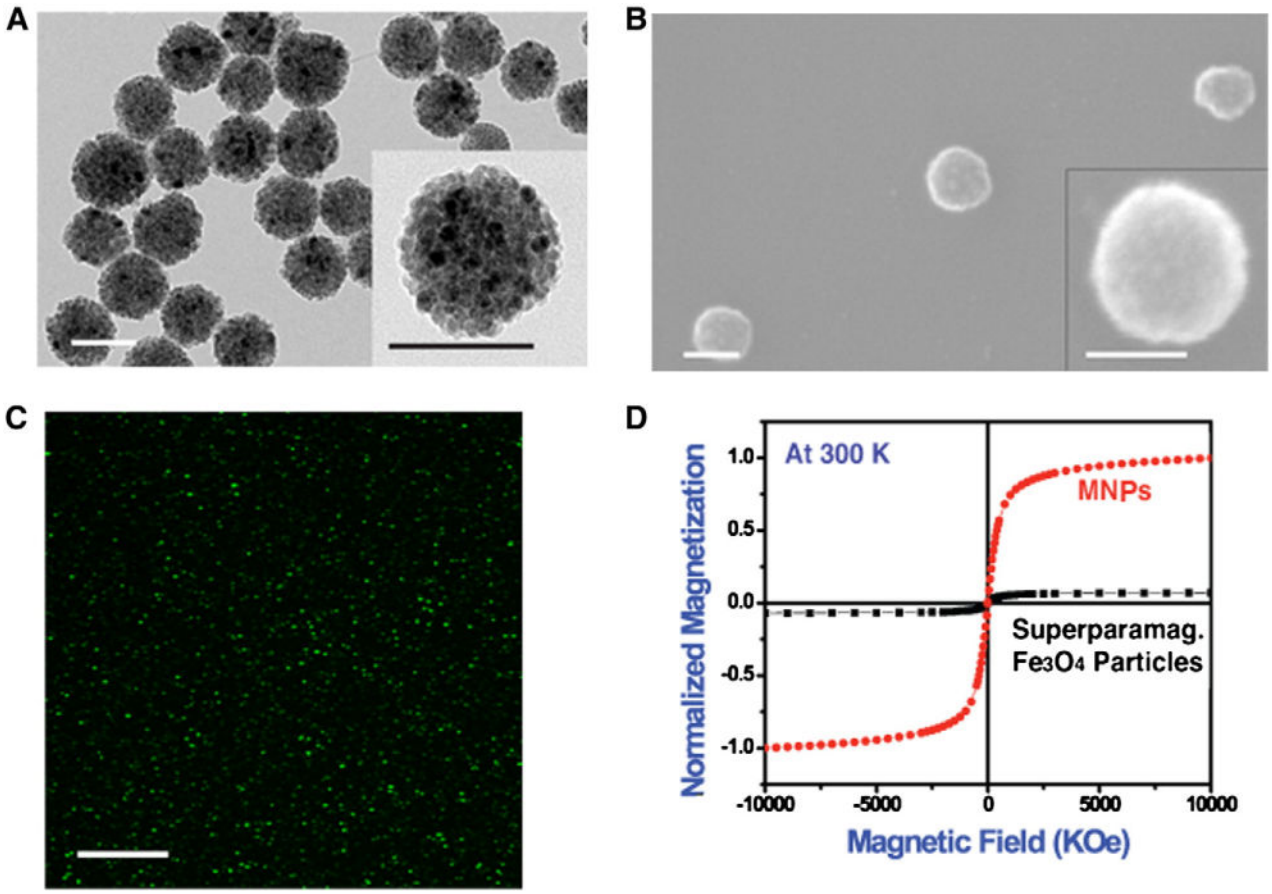


**Fig. 1.**

Characterization of fluorophore labeled MNPs. (A) TEM micrograph showing trapped magnetic nanoparticles in MNPs. (B) SEM micrograph showing the MNP size and shape. (C) Confocal microscopy images of the nanoparticles (green colored fluorophore, 9,10-bis(phenylethynyl)-anthracene, are embedded in MNPs). (D) M–H loops showing a significant increase in magnetic moment in MNP configuration as compared with isolated 10 nm magnetic nanoparticles of $Fe_3O_4$. Scale bar, 100 nm (A,B), 50 μm (C).

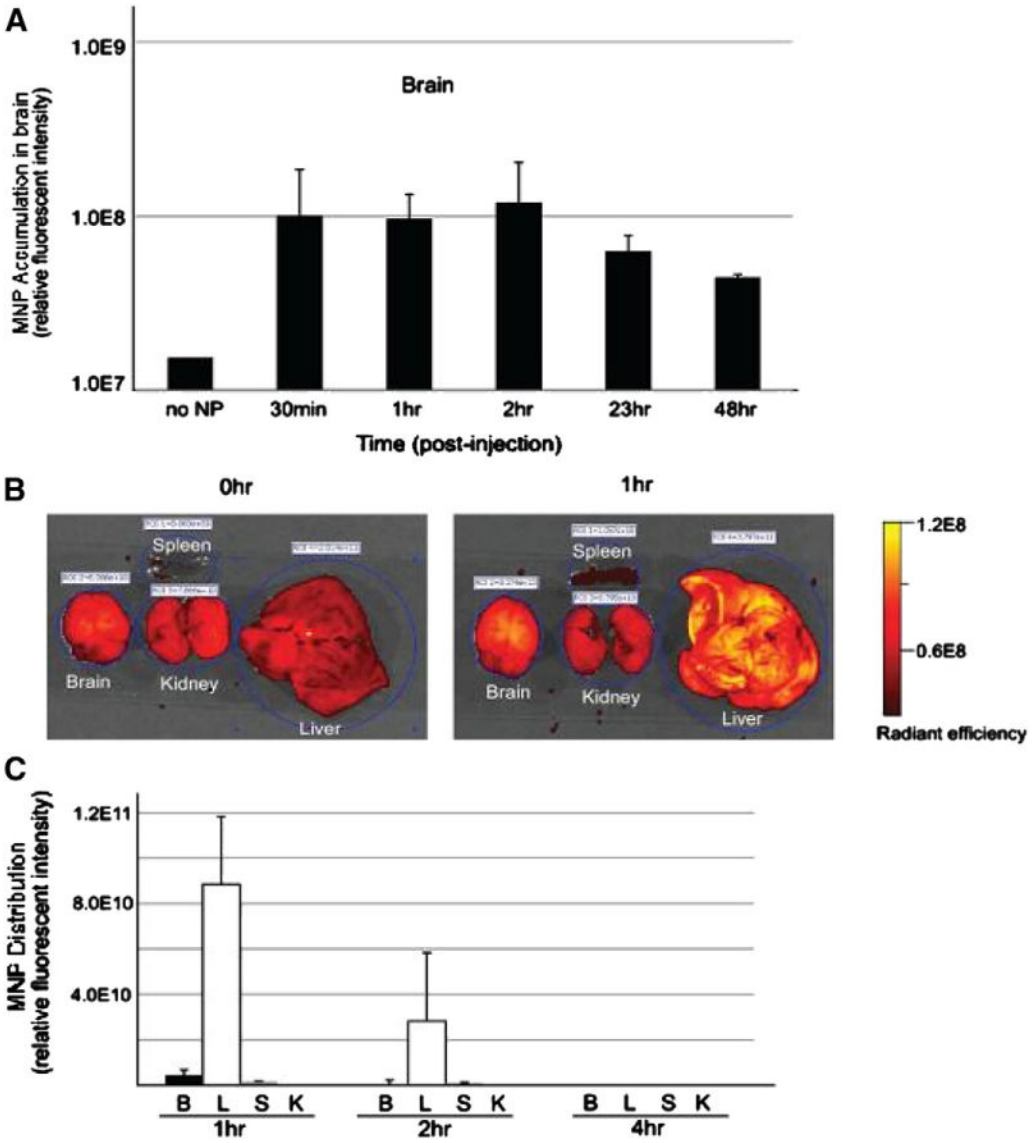


**Fig. 2.**

Biodistribution of MNPs. (A) In vivo accumulation of intravenously injected anthracene labeled MNPs in the brain reached its peak levels as early as 15–30 min to 2 h post-injection and then slowly diminished over time. (B) Biodistribution of MNPs in various organs measured at 1 h post-injection. A large fraction of MNP was found in the liver. (C) Relative distribution of MNPs from each organ (B—brain, L—liver, S—spleen, K—kidney) after 1, 2, and 4 h incubation is quantitated. Error bar, standard deviation.

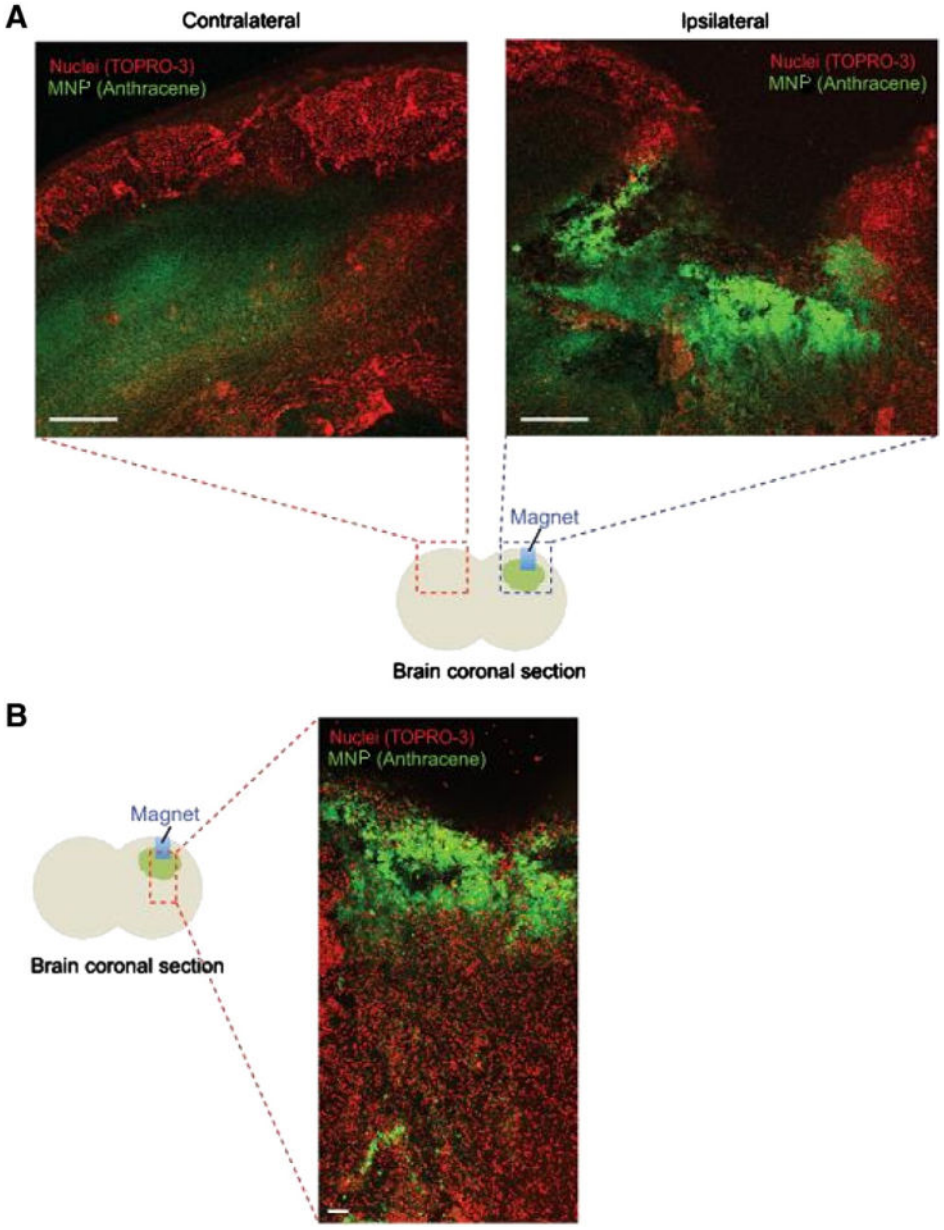


**Fig. 3.**

Magnetically vectored MNPs accumulate in the brain. (A) Small magnet was implanted in the right hemisphere of mice by stereotactic injection. (Blue represents the inserted magnet and green shade represents MNPs in cartoon). One week after implantation, MNPs were administered by intravenous injection. Confocal analysis demonstrates accumulation of MNPs in the ipsilateral hemisphere whereas background level of MNPs was found in the contralateral hemisphere. Staining of cell nuclei was observed with TO-PRO-3. Scale bar: 500 μm. (B) Confocal analysis of coronal sections of brain demonstrates enrichment of the MNPs near where the magnet was placed. Scale bar: 100 μm.

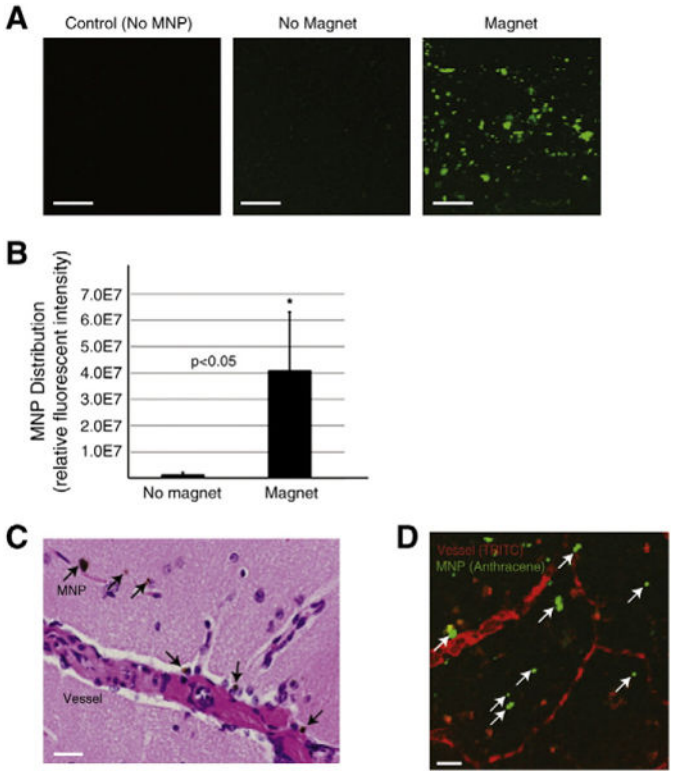


**Fig. 4.**

External magnetic force enhances BBB crossing and perivascular accumulation of MNPs in brain. (A) Confocal analysis demonstrates accumulation of MNPs in the brain facilitated by the application of external magnetic force (Nd–Fe–B magnet near the skull). Representative images of brain sections from a mouse with no MNP (left), injected with MNP but without applied magnetic field (middle) and injected with MNPs and with applied external magnetic field (right) are shown. (B) Quantitative measurements of relative fluorescent intensity of each brain section from panel (A) are shown. The delivery of MNPs is enriched by 26-fold when magnetic field was applied. Error bar indicates standard deviation ($p<0.05$, Wilcoxon rank sum test, two-sided). (C) Hematoxylin and eosin staining of the brain sections demonstrate perivascular accumulation of MNPs (arrow) in the cortex of the brain. (D) Confocal microscopy image of vessel (perfused with TRITC–dextran, red) and MNPs (labeled with fluorophore, green) demonstrates extravasation of MNPs. Scale bar, 20 μm (A,C), 50 μm (D).

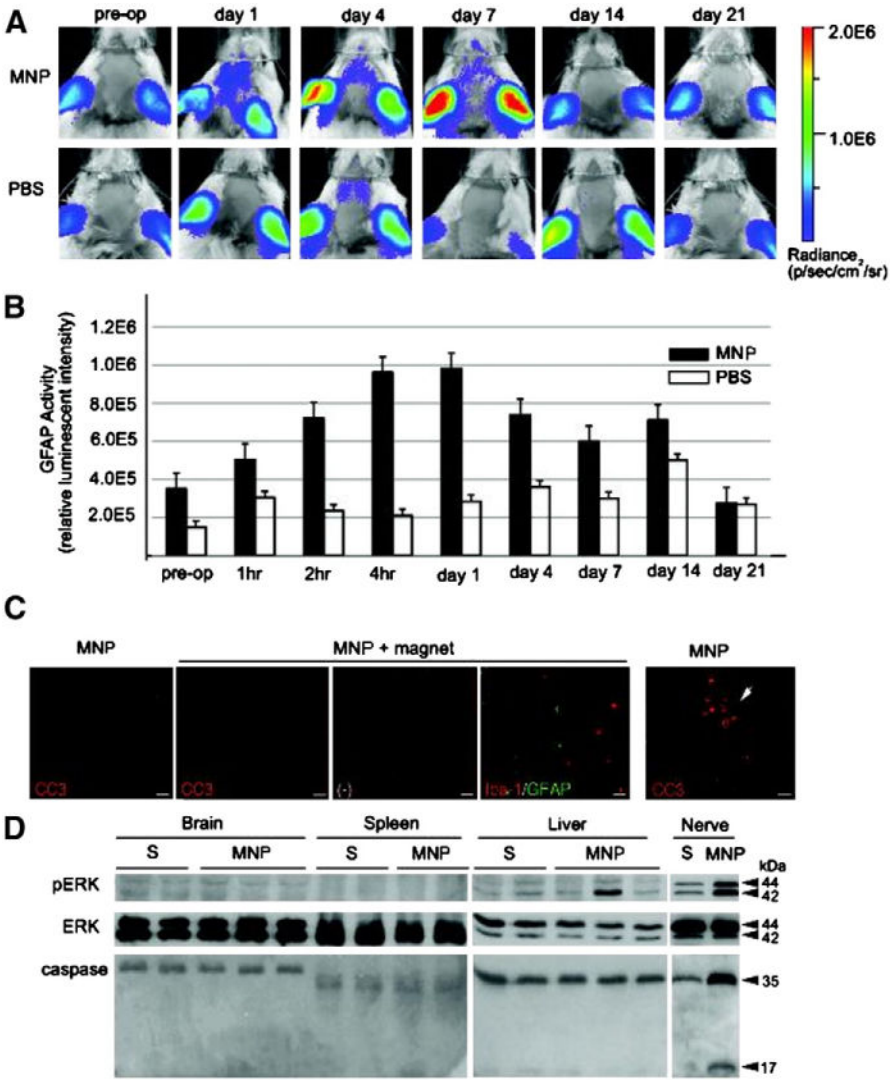


**Fig. 5.**

MNP administration produced no acute or long-term toxicity in vivo. (A) GFAP activity (measured by luciferase activity) increased after the injection of MNPs, reached its peak at 24 h after injection, and decreased over time. (B) MNP-mediated astrogliosis was quantified at each time point. (C) Cleaved caspase 3 (red), or control Iba-1 (red)/GFAP (green) immunofluorescence in the brain 1 h post MNP or PBS (S) injection, with and without magnet is shown. Nerve exposed MNP was used for positive control (arrow). Scale bar: 50 μm. (D) Western blotting for pERK, ERK and caspase 3 of the brain, spleen and liver of GFAP-luc mice, 4-week post MNP or control intra-neural MNP injection.

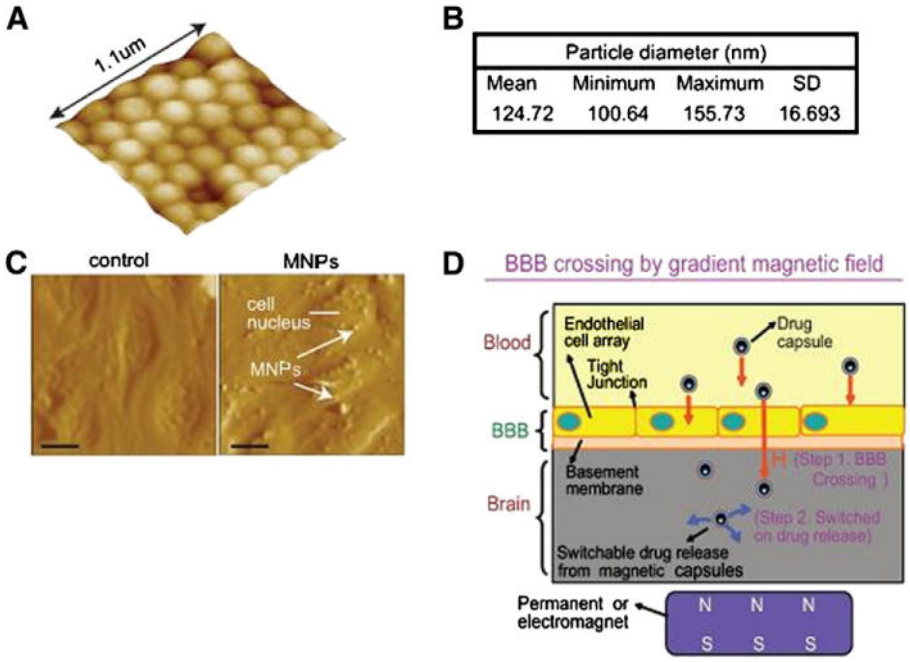


**Fig. 6.**

MNPs uptake by endocytosis into human brain endothelial cells. (A) AFM imaging of MNPs dried on functionalized mica substrate. (B) MNP size distribution. (C) Cells before (left) and after (right) applying the MNPs, endothelial uptake of MNPs (right, arrows) are shown. Scale bar: 20 μm. (D) Schematic illustration of the extravasation of magnetic nanocapsules (MNCs). Translocation of MNCs via DC gradient magnetic field is processed first, followed by switchable drug release inside the brain parenchyma.

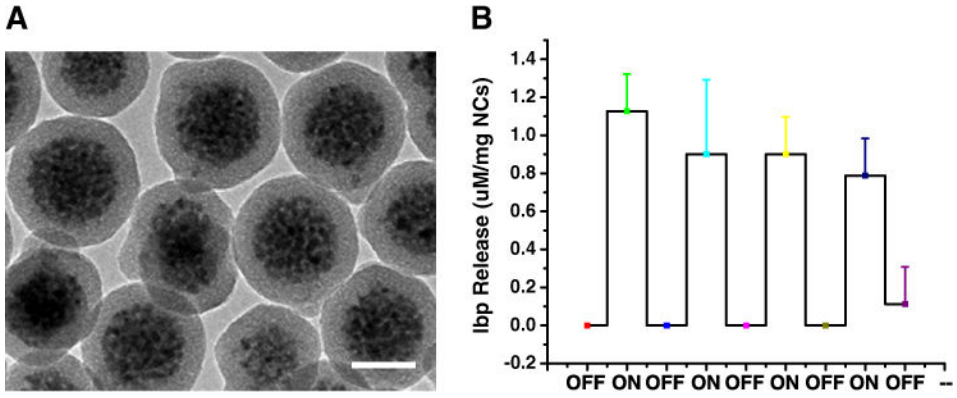


**Fig. 7.**

On-demand drug release from SiMNCs. (A) TEM image showing trapped magnetic nanoparticles inside SiMNCs. Scale bar: 100 nm. (B) On–Off switchable release from ibuprofen (Ibp)-containing SiMNCs by RF magnetic field on–off cycling.